Scientific Reports

https://doi.org/10.1038/s41598-026-44269-y

Article in Press

Ground control strategies for longwall top-coal caving panel in extra-thick coal seams with thick-hard roof

Received: 16 September 2025

Accepted: 10 March 2026

Published online: 17 March 2026

Cite this article as: Wang R., Zhang W., Wang H. *et al.* Ground control strategies for longwall top-coal caving panel in extra-thick coal seams with thick-hard roof. *Sci Rep* (2026). https://doi.org/10.1038/s41598-026-44269-y

Rui Wang, Wei-guang Zhang, Hao-sen Wang, Zai-jiang Yu & Qiang Zhang

Ground control strategies for longwall top-coal caving panel in extra-thick coal seams with thick-hard roof

Rui WANG[1,*], Wei-guang ZHANG[1], Hao-sen WANG[2,*], Zai-jiang YU[1], Qiang ZHANG[3]

[1] Key Laboratory of Xinjiang Coal Resources Green Mining, Xinjiang Key Laboratory of Coal-bearing Resources Exploration and Exploitation, Xinjiang Engineering Research Center of Green Intelligent Coal Mining, Xinjiang Institute of Engineering, Urumqi 830023, China
[2] School of Geology and Mining Engineering, Xinjiang University, Urumqi, 830047, China
[3] School of Mines, China University of Mining and Technology, Xuzhou, 221116, China

Corresponding author: Rui Wang (e-mail: rwang@cumt.edu.cn); Haosen Wang (e-mail: wanghaosen@xju.edu.cn).

ABSTRACT Thick-hard roof fracturing presents a significant challenge for disaster prevention in longwall mining. This study investigates the 15311 south working face and develops a mechanical model to analyze energy release during both initial and cyclic roof fracturing, along with the associated disaster mechanisms. Results indicate that total energy release increases with mining depth, roof thickness, and tensile strength, but decreases with the thickness of the immediate roof. The energy released during initial main roof fracturing is more than twice that of cyclic fracturing. Based on site geology, directional long-drilling fracturing parameters for the thick-hard fine sandstone roof were determined, with a single-point water injection of 20 m³ and a fracturing point spacing of 15 m. Following the "energy mitigation–structural weakening–stress regulation" principle, a "fixed-length drilling–hydraulic fracturing" model was implemented. On-site monitoring showed maximum movements in the tailgate of 236 mm in coal pillar gangs, 135 mm in solid coal, and 287 mm in roof-floor convergence. The initial pressure step decreased from 45 m to 18 m, and average cyclic pressure steps were reduced by 35% compared with a non-fractured face. The proposed scheme effectively facilitated safe and efficient mining under a thick–hard roof.

Keywords Extra-thick coal seams, thick-hard roof, fully mechanized top-coal caving mining, large-section mining space, directional hydraulic fracture.

1. INTRODUCTION

During large-scale, high-intensity longwall mining, safely and efficiently advancing working faces under thick-hard roofs remains a global challenge [1-2]. In the recoverable reserves of thick coal seams in China, the proportion of uniaxial compressive strength of the roof rock strata that exceeds 60 MPa reaches 37%. This corresponds to more than 1,200 longwall workings, most of which are distributed in large-scale production mines, such as Datong in Shanxi, Shaanxi, Mongolia [3,20]. Owing to their high integrity, strength, and self-stabilization capacity, these hard roofs are prone to forming large, overhanging sections in the open area during longwall advancement, with the associated hazards strongly influenced by geological conditions and mining parameters[4,5]. Relevant studies have shown that when the length of the suspended roof exceeds 1/3 of the working face length, the elastic strain energy accumulated in the roof plate can reach the order of 10^9J, and the risk of dynamic hazards, such as impact ground pressure and hurricane effects, increases significantly [6-7]. In addition, the convergence and closure rate of the roadway triggered by the overhanging roof of the thick-hard top plate can be up to 3~5 times greater than under conventional geological conditions, and the rate of hydraulic bracket crushing and destruction is elevated to 22%~35%, factors significantly limiting the safe and efficient mining of underground coal longwalls [8,9,22,23].

Researchers at home and abroad have used multiple means to carry out in-depth research on the mechanism of hard roof disasters and technology to control them, and achieved good results in field application. Dou et al. based on the principle of static and dynamic load superposition, analyzed the mechanisms of preventing impact pressure and achieving control of the hard roof and proposed technology for the time-sharing, zoning, and grading of broken roof blasting prevention and control [10]. Based on large quarries, Yu et al. revealed the breaking mechanism of hard top plates in near and far fields and proposed the use of integrated hydraulic fracturing joint prevention and control technology in the Datong mine area in China, which has been verified [11]. Kang et al. established a fracture network evolution model for the hydraulic fracturing of a thick-hard sandstone roof based on the fracture expansion energy criterion and proposed the use of "graded pressure boosting-directional injection", which shortened the step interval of the roof cycle from 32 m to 16 m [12,20]. Zhao et al. obtained inversion results based on micro-seismic CT. When the spacing of fracturing sections is >50m, the connectivity of the fracture network is less than 60%, which leads to the "island effect" in the weakened area [13,19]. Based on fracture mechanics and discrete element numerical simulation, Ju et al. analyzed the asymmetric expansion of hydraulic fracture cracks in laminated sandstone roof and proposed the "critical stress difference ratio" as a parameter for predicting the direction of hydraulic fracture expansion [14]. Based on a three-point bending experiment

performed on half discs and theoretical fracture mechanics analysis, Zhao et al. investigated the influence of the cutting angle on the direction of expansion of hydraulic fracture cracks in roof, providing key information for determining the time of hydraulic fracturing and anti-punching in hard roof [15,21].

The above studies provide a reliable theoretical foundation and technical reference for understanding the mechanisms and controlling disasters caused by overhanging roofs under thick, hard roof slabs. However, previous research exhibits notable limitations in the design of directional hydraulic fracturing parameters for hard rock formations. In particular, fracture point spacing and propagation range were often determined based on field experience or laboratory tests. Alternatively, the strength reduction method was applied in engineering-scale modeling to analyze the control effect of hydraulic fracturing on the roof, yet such numerical models were insufficient to accurately assess the degree of hard roof weakening or its impact on the mining process in detail[22,23]. Consequently, there remains a lack of engineering-scale numerical models capable of evaluating both the extent of roof weakening due to hydraulic fracturing and its effect on mining operations.

In response, this study develops a mechanical model of a hard roof in a longwall face, using the 15311 south workings of a mine as a case study. An analytical solution is derived for the total energy released during hard roof fracture, and a sensitivity analysis of its influencing factors is performed. To reduce the length of the overhanging roof and minimize the energy released from hard roof failure, this study proposes a hydraulic fracturing control strategy using fixed-length drilling holes for thick, hard roof plates. The approach was successfully implemented at the research site, providing a valuable reference for future studies in this field.

2. CASE STUDY

Xinjiang Coking Coal Group 1890 Coal Mine, located within Dabancheng District, Urumqi City, is situated approximately 130 km north of Urumqi City, as shown in Figure 1. The mine has an annual production capacity of 1.20 Mt/a. Within the mine field, the coal seams are primarily concentrated in the Lower Jurassic Badaowan Formation, which contains a total of 12 minable coal seams. The current production area is the first level of the third mining district, which operates one coal mining face and two development headings. The 15311 south working face is located within the first level third mining district. It is bounded by the outcrop of the 5# coal seam to the east, the 15312 working face to the west, the southern mine field boundary protective coal pillar to the south, and the 1901 east small shaft and 1901 west small shaft to the northeast. The 15311 south working face has an average dip length of 275 m and an average strike length of 988 m, as shown in Figure 1(b). The main mining target is the 5# coal seam, which has an average minable thickness of 27.15 m and an average dip angle of 2°. The lithology of the seam roof, from bottom to top, consists sequentially of sandy mudstone, fine sandstone, carbonaceous mudstone (or coaly shale), sandy mudstone, and fine sandstone. A comprehensive columnar section of the roof and floor strata is shown in Figure 1(a). In situ uniaxial compressive strength tests on the roof strata above the coal seam were conducted using a WQCZ-56 in situ rock strength tester. The test results are shown in Figure 1(c). The borehole was positioned perpendicular to the roof of the 15311 south working face haulage roadway, with a depth of 50 m. The vicinity of the borehole collar corresponds to the 5# coal seam, where the compressive strength ranges between 22 and 32 MPa. The peak strength of the fine sandstone roof beyond 35 m from the collar exceeds 70 MPa, classifying it as a hard rock layer.

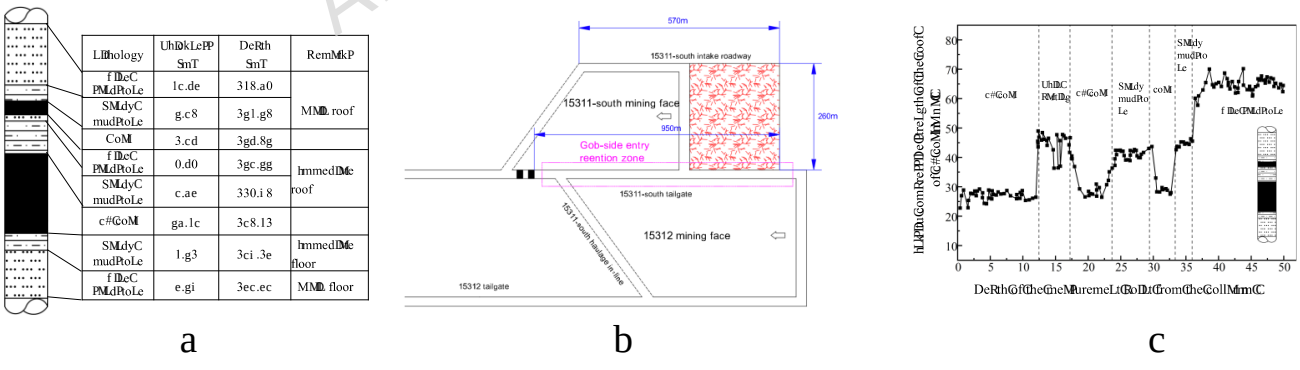

FIGURE 1. Engineering geological conditions.

The currently mined 5# coal seam at the 1890 Coal Mine of Xinjiang Coking Coal Group is overlain by a unique multi-layered hard roof strata structure, exhibiting intense ground pressure characteristics typical of thick, hard, and difficult-to-cave roof strata. Affected by this intense ground pressure, the surrounding rock of the 15311 south working face roadway has suffered severe deformation and damage. This has primarily manifested as intense floor heave driving “inverted trapezoidal” convergence in both ribs, with convergence typically exceeding 1.0 m. Influenced by the multi-layered hard roof structure, the surrounding rock periodically exhibits dynamic failure characterized by “sudden displacement”, leading to instability in the surrounding rock and extensive failure of the support structure. The characteristics of the roadway deformation and damage are shown in Figure 2.

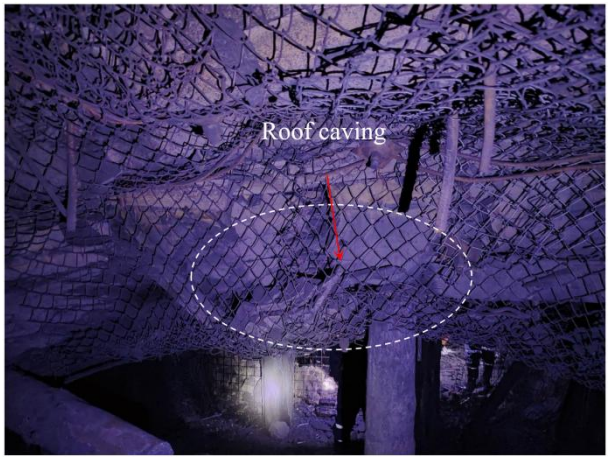

FIGURE 2. The characteristics of roadway deformation and damage.

3. THE EFFECT OF A THICK-HARD OVERHANGING ROOF IN LONGWALL QUARRIES AND ITS DISASTER-CAUSING MECHANISM

3.1 SUSPENDED ROOF EFFECT OF THICK-HARD MAIN ROOF

During the advancement of a longwall working face, the soft immediate roof (or top coal) can usually collapse in time in the mining void area due to the low strength of the rock strata and the development of joints and fissures under the coupling effect of mining stress and self-weight. Due to the thick-hard roof with high strength and good integrity, it resists sliding down under the action of the overlying rock layer and self-weight, forming a large overhanging roof in the open area. With further advancement of the working face, the overhanging main roof bending moment reaches its limit state, resulting in O-X cycle fracturing, as shown in Figure 3.

A large amount of elastic strain energy accumulates inside the thick-hard roof before breaking, and the strain energy is suddenly released after its rupture, which seriously threatens the safety of mining equipment and operators. A suspended roof disaster undergoes a three-stage evolution characterized by "energy accumulation–structural instability-power release", as shown in Figure 4.

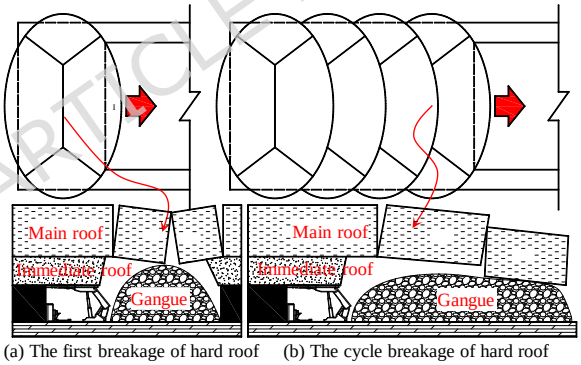

(a) The first breakage of hard roof (b) The cycle breakage of hard roof

FIGURE 3. Fracture characteristics of the thick–hard roof overlying the mining area

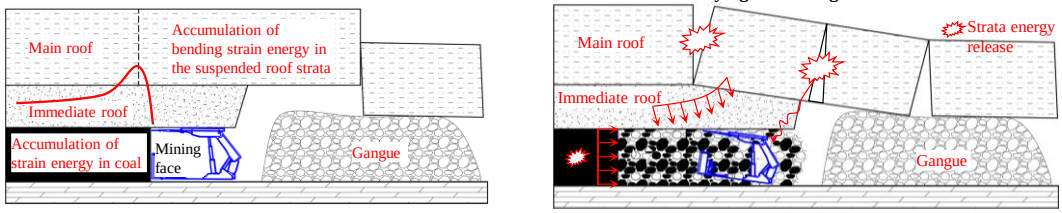

(a) Accumulation of bending strain energy in roof. (b) Accumulation of breaking strain energy in roof.

FIGURE 4. Schematic diagram of disaster mechanisms induced by thick-hard roof fracture.

3.2 DISASTER MECHANISM OF THICK-HARD SUSPENSION ROOF FRACTURING

This study shows that as the working face advances, the thick-hard roof breaks and releases energy to form a dynamic shock wave in the overhanging roof of the hollow area, which is dynamically transmitted to the vicinity of the working face and superimposed with the high static load of the coal and rock body, further inducing an impact ground pressure disaster. Therefore, it is necessary to establish a mechanical model of thick and hard roof fracturing, as shown in Figure 5, to analyze

the energy accumulation characteristics of thick and hard roofs and their influencing factors, so as to provide theoretical support and data support for the management of thick and hard overhanging roof disasters.

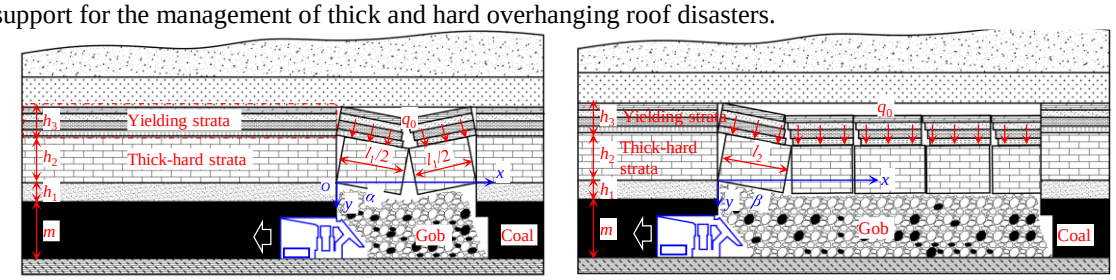

(a) Mechanical model for the initial fracture of hard roof. (b) Mechanical model for the cycle fracture of hard roof.

FIGURE 5. Mechanical model for the fracture of thick–hard roof.

According to the relevant principles of material mechanics, without considering the difference in the length direction of the working face, the thick-hard roof before the initial fracturing can be simplified as a solidly supported beam structure with unit width, and the thick-hard roof before the cycle fracturing can be simplified as a cantilever beam structure with unit width[24-26]. The bending moment M1(x) on any cross-section of the thick-hard roof before the initial fracturing, and the bending moment $M_2(x)$ on any cross-section of the thick-hard roof before cyclic fracturing can be expressed as,

$$\begin{cases} M_1(x) = \dfrac{q_0}{12}\left(6l_1x^2 - 6x^2 - l_1^2\right) \\ M_2(x) = -\dfrac{q_0}{2}\left(l_2 - x\right)^2 \end{cases} \tag{1}$$

In Eq. (1), l_1 is the initial fracturing step of the thick-hard roof, m; l_2 is the cycle fracturing step of the thick-hard roof, m; and q_0 is the overlying load of the thick-hard roof, N/m.

With the tensile strength as its breaking limit, the initial fracturing step l_1 and cycle fracturing step l_2 of the thick-hard roof are calculated:

$$\begin{cases} l_1 = h_2\sqrt{\dfrac{2R_t}{q_0}} \\ l_2 = h_2\sqrt{\dfrac{R_t}{3q_0}} \end{cases} \tag{2}$$

In Eq. (2), h_2 is the thickness of the thick-hard roof, m; R_t is the tensile strength of the thick-hard roof, MPa.

According to the relevant principles of elastic mechanics, the thick-hard roof is regarded as an elastic rock beam, and its bending strain energy, U, before breaking can be expressed as:

$$U = \frac{1}{2EI}\int\left[M(x)\right]^2 \mathrm{d}x \tag{3}$$

In Eq. (3), E is the modulus of elasticity of the thick-hard roof, GPa; I is the moment of inertia per unit width of the thick–hard roof beam section, $I = h_2^2/12$.

Substituting Eq. (1) into Eq. (2), the bending strain energy released by the initial fracturing and cyclic fracturing of the thick-hard roof can be obtained as:

$$\begin{cases} U_{11} = \displaystyle\int_0^{l_1} M(x)\mathrm{d}x = \frac{l_1^5 q_0^2}{120Eh_2^3} \\ U_{21} = \displaystyle\int_0^{l_2} M(x)\mathrm{d}x = \frac{3l_2^5 q_0^2}{10Eh_2^3} \end{cases} \tag{4}$$

In Eq. (4), U_{11} and U_{21} are the bending strain energy released by the initial and cyclic fracturing of the thick-hard roof, respectively, in kJ.

The rotational kinetic energy brought about by the initial and cyclic fracturing of the thick-hard roof (U_{12} and U_{22}, respectively) and its overlying loaded rock layer with its common movement are as follows:

$$\begin{cases} U_{12} = \dfrac{1}{4}\left(\rho_2 h_2 + \displaystyle\sum_{i=1}^{n}\rho_{3i}h_{3i}\right) g l_1^2 \sin\alpha \\ U_{22} = \dfrac{1}{2}\left(\rho_2 h_2 + \displaystyle\sum_{i=1}^{n}\rho_{3i}h_{3i}\right) g l_2^2 \sin\beta \end{cases} \tag{5}$$

In Eq. (5), g is the acceleration of gravity, N/kg; ρ_2 and ρ_{3i} are the densities of the thick-hard roof and overlying load layer, kg/m^3; h_{3i} is the thickness of the load layer of the thick-hard roof, m; n is the number of load layers of the thick-hard roof; and α and β are the slewing angles of the hard rock layer after the initial fracturing and cyclic fracturing, °, respectively.

According to the theory of mine pressure and rock layer control, the slewing angles α and β after breaking the thick-hard roof can be obtained from Eq. (6):

$$\begin{cases} \sin\alpha = \dfrac{2[m + h_1(1-k)]}{l_1} \\ \sin\beta = \dfrac{[m + h_1(1-k)]}{l_2} \end{cases} \tag{6}$$

In Eq. (6), k is the immediate roof breaking coefficient; ρ_2 and ρ_{3i} are the densities of the thick–hard roof and the overlying load layer, respectively, kg/m^3; h_1 is the thickness of the immediate roof, m; and m is the thickness of the coal seam mined, m. The total energy released after the initial breaking of the thick-hard roof and the cycle breaking of the load layer is determined as follows.

From the above analyses, it can be seen that the total energy released after the initial fracturing of the thick-hard roof and the cyclic fracturing and the load layer after the coordinated slewing and stabilization of the thick-hard roof are, respectively,

$$\begin{cases} U_1 = U_{11} + U_{12} = \dfrac{l_1^5 q_0^2}{120Eh_2^3} + \dfrac{1}{2}gl_1\left(\rho_2 h_2 + \sum_{i=1}^{n}\rho_{3i}h_{3i}\right)[m + h_1(1-k)] \\ U_2 = U_{21} + U_{22} = \dfrac{3l_2^5 q_0^2}{10Eh_2^3} + \dfrac{1}{2}gl_2\left(\rho_2 h_2 + \sum_{i=1}^{n}\rho_{3i}h_{3i}\right)[m + h_1(1-k)] \end{cases} \tag{7}$$

From Eq. (7), it can be seen that the total energy released after hard roof fracturing is closely related to the thickness of the hard roof, h_2; the modulus of elasticity of the hard roof, E; the fracture step of the hard roof, l_1 and l_2; the overburden load of the hard roof, q_0; the mining thickness of the coal seam, m; the thickness of the immediate roof, h_1; and the coefficient of expansion of the immediate roof, k. The higher the total energy released by the fracturing of the hard rock layer, the greater the energy of the dynamic load stress wave transmitted to the working face, and the greater the risk of impact damage to the working face.

The higher the total energy released by the fracture of the hard rock layer, the higher the energy of the dynamic load stress wave transmitted to the working face, and the higher the risk of impact damage to the working face. When it reaches the index of its impact instability, the working face is highly likely to produce strong impact ground pressure, which can damage equipment and cause casualties in serious cases, as shown in Figure 6.

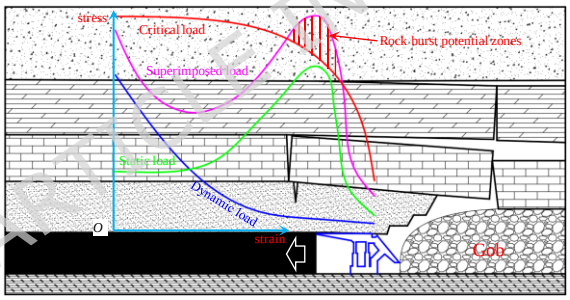

FIGURE 6. Criterion for the generation of rock burst.

3.3 ANALYSIS OF INFLUENCING FACTORS AND IMPACT MECHANISM ON TOTAL ENERGY RELEASE DURING THICK-HARD ROOF FRACTURE

Table 1 shows the results of the relevant parameters from the laboratory test, the geological conditions of the working face site, and field measurement results. Substituting the relevant parameters into Eq. (2), it can be determined that the initial fracturing step, l_1, of the thick-hard roof of the 15311 south working face is 60.14 m, and the cycle fracturing step, l_2, is 24.55 m.

TABLE I

PHYSICAL AND MECHANICAL PARAMETERS AND GEOMETRIC CHARACTERISTICS OF COAL AND ROCK MASS.

Influencing Factors	Variables	Value
The thickness of immediate roof	h_1	12.28 m
The density of hard roof	ρ_2	2500 kg/m^3
The elastic modulus of hard roof	E	6.4 GPa
The thickness of hard roof	h_2	15.46 m
The mining height of coal seam	m	27.15 m
Overburden load on hard roof	q_0	600 kPa
The tensile strength of hard roof	R_t	4.54 MPa
The bulking factor of immediate roof	k	1.2
The density of overburden strata	ρ_{3i}	2400 kg/m^3
The thickness of overburden strata	h_{3i}	14.56 m

Using the single-control-variable method, sensitivity analyses were carried out on the patterns of influence of different factors on the total energy released after breaking the thick-hard roof, as shown in Figures 7 and 8.

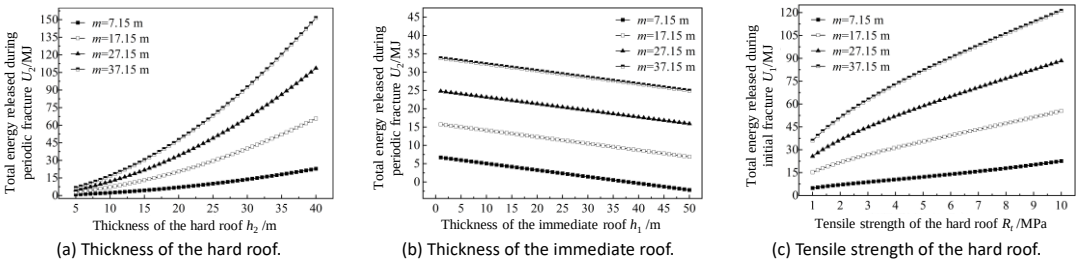

(a) Thickness of the hard roof. (b) Thickness of the immediate roof. (c) Tensile strength of the hard roof.

FIGURE 7. Influencing factors of total energy released by initial fracture of the hard roof.

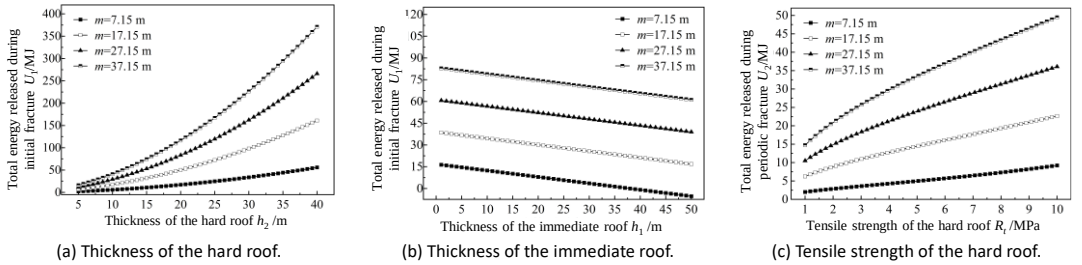

(a) Thickness of the hard roof. (b) Thickness of the immediate roof. (c) Tensile strength of the hard roof.

FIGURE 8. Influencing factors of total energy released by periodic fracture of hard roof.

(1) From Figures 7 and 8, it can be seen that the total energy released by the thick-hard roof fracturing is positively correlated with the mining thickness of the coal seam and the thickness of the thick-hard roof, and the tensile strength of the thick-hard roof and is negatively correlated with the thickness of the immediate roof; in the same geological context, the total energy released by the initial fracturing of the main roof is more than twice that released by the cyclic fracturing of the main roof.

(2) The greater the thickness of the thick-hard roof, the higher the elastic strain energy accumulated by its bending deformation, the higher the tensile strength, the larger the initial and cyclic fracturing, and the higher the total energy released by the fracturing of the unit width of the hanging roof.

(3) The smaller the immediate roof thickness and the larger the coal seam mining thickness, the lower the filling degree of immediate roof collapse and swelling in the gob area, the larger the slewing angle of the thick-hard roof after its initial and cyclic breaking, and the higher the slewing kinetic energy released by its slewing and stabilization with the overlying load.

(4) The greater the thickness of the immediate roof, the farther the thick-hard rock fracturing location is from the working face, the greater the attenuation of the dynamic load stress wave generated by the fracturing transmitted to the vicinity of the working face, and the lower the risk of the working face generating impact ground pressure.

In engineering practice, hydraulic fracturing and other measures can be used to weaken the integrity of the internal structure of the hard rock layer, prompting it to collapse in the open area in time after the working face is mined back to reduce its suspended roof. This allows part of the elastic strain energy to be released gradually and safely, avoiding the impact triggered by the sudden large-scale fracture of the roof to focus on the release of high energy. In addition, corresponding water injection and softening measures can be applied to the weakened roof below to improve its risk of release, degree of crushing, and degree of filling in the extraction zone. This not only reduces the slewing space of thick-hard roof fracturing but also improves the attenuation coefficient of the dynamic load stress wave formed by the fracturing of the thick–hard roof in the soft and weak rock layer below.

4. HYDRAULIC FRACTURING IN FIXED-LENGTH BOREHOLES IN THE FIELD

4.1 PRINCIPLES OF HYDRAULIC FRACTURING WITH FIXED-LENGTH DRILLING

After setting up the directional drilling equipment and inserting the fracturing tool string into the designated location, the target layer is fractured using single-card fracturing through double packers, with the high-pressure pump activated. When the water pressure reaches the start-up pressure of the rear packer, a sealed space is formed between the packers. As the pumping pressure continues to increase, high-pressure water is injected into the sealed space, gradually increasing the pressure acting on the borehole wall[27-30]. When the water pressure exceeds the fracture pressure of the rock formation, rupture cracks develop along the borehole wall, compromising the overall integrity of the rock. Upon completion of the first fracturing operation, the high-pressure pump is turned off, the packer automatically returns to its original size, and the directional drilling rig moves the packer to the next position for the subsequent fracturing. Each designed construction section is fractured in sequence, and the adjacent sections combine to form a three-dimensional, continuous crack network in the rock formation. The process flow of hydraulic fracturing with fixed-length drilling is illustrated in Figure 9.

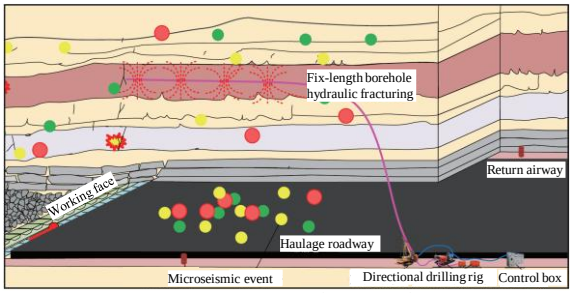

(a) Schematic diagram of hydraulic fracturing process via directional long boreholes in thick–hard roof.

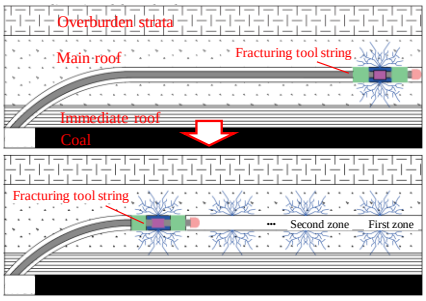

(b) Construction schematic of staged hydraulic fracturing in a single borehole.

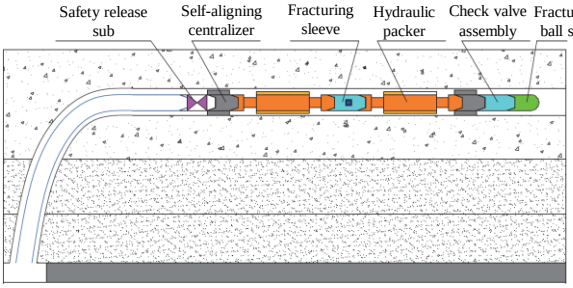

(c) Structural schematic diagram of fracturing tool string.

FIGURE 9. Principle of directional long borehole hydraulic fracturing technology.

4.2 HYDRAULIC FRACTURING TOP CUTTING AND PRESSURE RELIEF PROGRAM

Based on comprehensive theoretical calculations, numerical simulation results, the geological conditions of the working face, and fracturing parameter design principles, according to the recoverable length of the 15311 south working face, a technical scheme for hydraulic fracturing with fixed-length drilling holes for the 15311 south working face was determined, as shown in Figure 10, alongside the technical parameters of the directional drilling holes, as shown in Table 3.

(1) According to the actual production conditions, the 1# and 2# drilling sites were arranged, which are located in the backwind link of the 15311 south intake roadway (H1, H2, L1, L2, L3, M1, M2 drilling holes) and in the 15312 tailgate (H3, H4, L4, L5, L6), respectively.

(2) According to the rock layer histogram, the fixed-length drill holes were divided into three layers 6 m, 15 m, and 48 m above the roof of the roadway.

(3) The diameter of the drill holes was 120 mm, and there were four high-level drill holes (48 m level) (H1, H2, H3, H4) located in the middle of the fine sandstone of the main roof; six low-level drill holes (15 m level) (L1, L2, L3, L4, L5, L6) located in the gangue position of the coal seam; and two supplemental holes (6 m level) in the shadow area of the turning radius of the fixed-length drill holes (M1, M2).

(4) The following conditions were used: H-type drilling design feed, 2772m; drilling influence range for 15311 south intake roadway to the working face direction, 50 ~ 210m, spacing 50m; L-type drilling design feed, 4134m; drilling influence range for 15312 tailgate to the working face direction, 30 ~ 230m, spacing 40m; M-type drilling design feed, 315m; drilling control range for 15312 tailgate to the working face direction, 106 ~ 131m, spacing of drilling, 131m; spacing of drill holes, 25m; and final position of drill holes crossing the stopping line, 20m.

(5) The spacing of the drilling holes was set at 1.0m, the height of the drilling holes was controlled at 1.8~2.0m from the bottom plate, the azimuth angle of the drilling holes was controlled within the range of ±3° according to the design requirements, and the inclination angle was controlled within the range of ±1° according to the design requirements, avoiding the influence of the anchor rods and anchor cables.

(6) According to the numerical simulation results and engineering experience, the backward segmental fracturing method was adopted to carry out segmental fracturing in a single borehole, and the spacing of fracturing points in the borehole was 15 m.

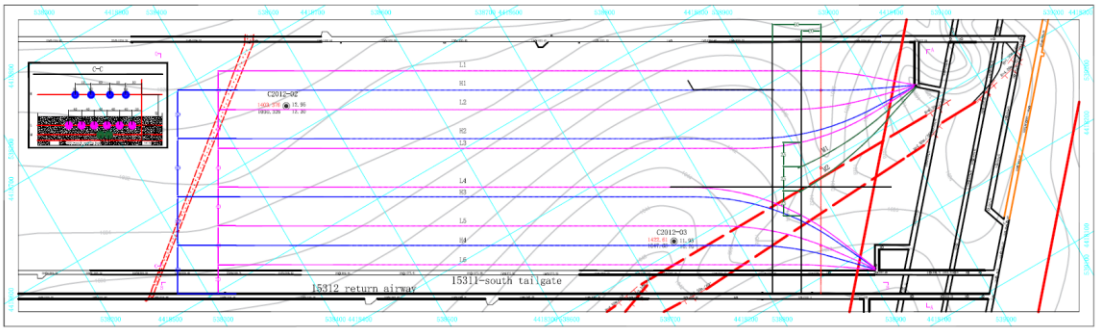

FIGURE 10. Directional hydraulic fracturing scheme for 15311 south working face.

TABLE 2

DESIGN PARAMETERS OF DIRECTIONAL HYDRAULIC FRACTURING IN 15311 SOUTH WORKING FACE.

Borehole number	Initial hole azimuth (°)	Initial hole dip angle (°)	Target azimuth (°)	Borehole diameter (mm)	Start point (m)	End point (m)	Fracturing stage (m)	Fracturing zone (m)
H1 Borehole	295.5	10	300.15	120	0	705	150-705	48m
H2 Borehole	272	10			0	717	162-717	
L1 Borehole	310.5	7			0	699	150-699	
L2 Borehole	284.5	7			0	705	150-705	15m
L3 Borehole	268	7			0	717	162-717	
M1 Borehole	260	10			0	150	-	6m
M2 Borehole	252	10			0	165	-	
H3 Borehole	335	10			0	681	126-681	48m
H4 Borehole	316	10			0	669	114-669	
L4 Borehole	338	7			0	681	126-681	
L5 Borehole	324	7			0	669	114-669	15m
L6 Borehole	304.5	7			0	663	108-663	

4.3 HYDRAULIC FRACTURING FIELD APPLICATION RESULTS

(1) Drill hole peeping in hard-top fractures

The internal integrity of the fractured borehole was analyzed using borehole imaging equipment, as shown in Figure 11. A through fracture was produced along the borehole axis near the fracturing point, and localized circumferential fissures were generated, which significantly reduced the integrity of the thick-hard roof (fine sandstone). As the working face advances, it is more likely to rapidly collapse into the void zone under the action of the overlying rock load and the hysteresis stress in the void zone.

FIGURE 11. Characteristics of thick–hard roof fracture before and after fracturing.

(2) Monitoring water injection pressure for fracturing in sections

Using the pressure monitoring equipment of the high-pressure water injection system, real-time tracking of the water injection pressure during the segmental fracturing process of the fixed-length borehole was carried out. Taking borehole H2 as an example, the water injection pressure curves at different fracturing stages are shown in Figure 12.

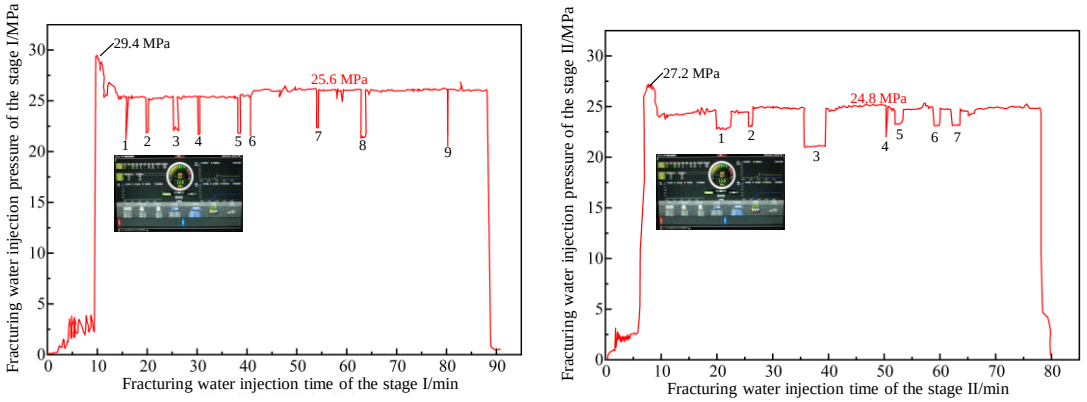

(a) Fracturing water injection pressure curve during stage I. (b) Fracturing water injection pressure curve during stage II.

FIGURE 12. Water injection pressure curve of directional hydraulic fracturing.

During the initial fracturing of each section of borehole H2, the water injection pressure showed fluctuations when the pressure reached about 3 MPa, which were caused by the continuous injection of high-pressure water into the sealer and the expansion of the sealer. Subsequently, the water injection pressure increased sharply and then continued to decrease, which indicates that the high-pressure water was continuously injected into the sealing interval between the packers at both ends, and the water pressure in the sealing interval increased to the fracturing pressure of the rock body, and the rock body on the surface of the borehole ruptured.

When the water injection pressure showed sawtooth-like fluctuations, it indicated that the water injection pressure entered the pressure preservation stage, and the hydraulic fractures continued to expand depth-wise; the presence of multiple pressure drops during the injection period indicated that the continuous injection of high-pressure water induced further rupture deeper in the rock body, and the hydraulic fractures expanded deeper away from the surface of the borehole, forming a network of penetrating cracks and dense hydraulic fractures, which achieved the effect of pre-fracturing.

In addition, the fracture initiation pressure, the water injection pressure, and the number of pressure drops during the first stage of fracturing were greater than those in the second stage. This indicates that the hydraulic fracture extension range produced by the first fracturing section was larger than the spacing between the two fracturing points, effectively weakening the hard top plate's integrity in the control range of the second fracturing section. Additionally, the two fracturing control ranges overlapped with each other, which further improved the control effect of hydraulic fracturing in directional long-distance drilling.

(3) Stress and deformation of roadway peripheral rock

A monitoring station was established every 50m in the 15311 south tailgate, and the station layout is shown in Figure 13(a). The surface displacement of the surrounding rock and the evolution of coal body stress in the 15311 south tailgate during the face mining period are shown in Figure 13(b). The deformation of the coal pillar gangs in the roadway started to increase at about 70m from the working face, the maximum distance of coal pillar gangs moving closer was 236 mm, the maximum distance of solid coal gangs moving closer was 135 mm, the maximum of roof and floor convergence was 287mm, and the roadway surface displacement was small enough to ensure the safe and efficient mining of the working face. After adopting directional long-drilling hydraulic fracturing in the 15311 south working face, the initial incoming pressure step in the working face was reduced from 45 m to 18 m; the incoming pressure steps in the upper, middle, and lower areas of the working face were reduced compared with that of the working face before hydraulic fracturing; and the average reduction in the cycle incoming pressure step was 35%. This technology effectively reduces overhanging of a thick-hard roof in an open area, reduces the pressure step in the working face, and ensures the safe and efficient mining of a longwall face under thick-hard roof.

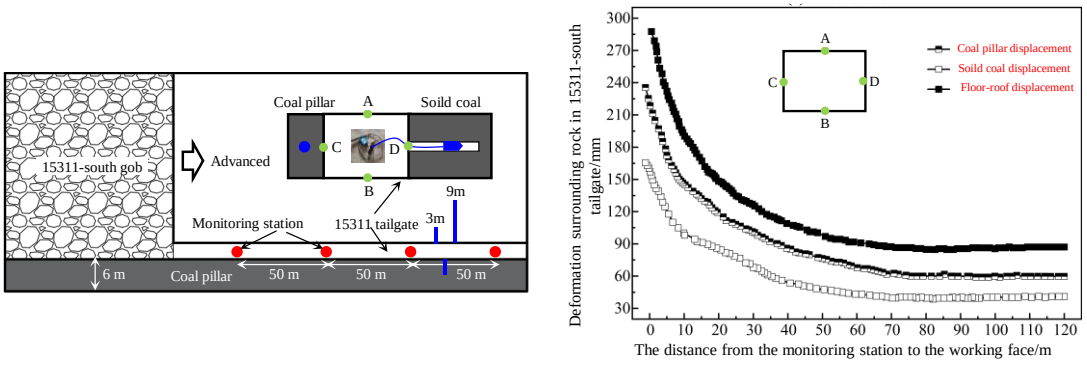

(a) Layout of the monitoring station (b) The law of deformation surrounding rock

FIGURE 13. Roadway deformation and coal stress monitoring curve.

5. CONCLUSION

(1) A mechanical model of a thick-hard roof in a longwall face was developed, and an analytical solution for the energy released during roof failure was derived. The total energy released is positively correlated with the coal seam mining thickness, the thickness of the thick-hard roof, and the roof's tensile strength, and negatively correlated with the thickness of the immediate roof. Notably, the energy released during the first main roof break exceeds twice that released during subsequent cyclic breaks.

(2) A control strategy based on hydraulic fracturing through long directional drill holes, with optimized key parameters, is proposed. Field implementation demonstrates that hydraulic fracturing significantly reduces the integrity of the thick–hard roof. During mining of the 15311 south working face, maximum movements were 236 mm in coal pillars, 135 mm in solid coal, and 287 mm in roof–floor convergence. Additionally, the initial pressure step decreased from 45 m to 18 m, and the average cyclic pressure step was reduced by 35% compared with an unfractured face, effectively ensuring safe and efficient longwall mining under a thick-hard roof.

Data Availability

The datasets used and/or analysed during the current study available from the corresponding author on reasonable request.

REFERENCES

[1] Z.G. Zhang, L.C. Dai, H.T. Sun, et al. Study on the spatiotemporal dynamic evolution law of a deep thick hard roof and coal Seam. *Processes*, vol. 11, no. 11, pp. 3173, 2023.

[2] B.B. Chen, C.Y. Liu, and B. Wang. A case study of the periodic fracture control of a thick-hard roof based on deep-hole pre-splitting blasting. *Energy Exploration & Exploitation*, vol. 40, no. 1, pp. 279-301, 2022.

[3] D. Zhang, J.B. Bai, R. Wang, et al. Investigation on instability mechanism and control of abandoned roadways in coal pillars recovery face: A case study. *Underground Space*, vol. 20, pp. 119-139, 2025.

[4] A.R. Chowdhury, S.C. Bakshi, A. Pramanik, et al. Design and study of lora-based iiot network for underground coal mine environment. *IEEE Access*, vol. 13, pp. 4984-4995, 2025.

[5] Z. Fan, X. Song, D. Wang, et al. Poroelastic solutions of a semi-permeable bore-hole under non-hydrostatic in situ stresses within transversely isotropic media. *Int. J. Geomech*. vol. 25, pp. 04024342, 2025.

[6] Q.W. Bu, M. Tu, X.Y. Zhang, et al. Analysis of energy accumulation and dispersion evolution of a thick hard roof and dynamic load response of the hydraulic support in a large space stope. *Frontiers in Earth Science*, vol. 10, pp. 884361, 2022.

[7] D. Zhang, J.B. Bai, Z. Tian, et al. Stability mechanism and control of the pumpable supports in longwall recovery room. *International Journal of Mining Science and Technology*, vol. 34, no. 7, pp.957-974, 2024.

[8] R. Gao, T. Kuang, X. Meng, et al. Effects of ground fracturing with horizontal fracture plane on rock breakage characteristics and mine pressure control. *Rock Mech. Rock Eng*. vol. 54, pp. 3229–3243, 2021.

[9] D.D. Qin, Z.C. Chang, and Z. Xia. Experimental study on the strain energy evolution mechanism of thick and hard sandstone roof in Xinjiang Mining Area. *Heliyon*, vol. 10, no. 2, pp. 24594, 2024.

[10] J.L. Jia, L.W. Cao, D.J. Zhang, et al. Study on the fracture characteristics of thick-hard limestone roof and its controlling technique. *Environmental Earth Sciences*, vol. 76, no. 17, pp. 605, 2017.

[11] R. Gao, B. Dou, B. Yu, et al. Ground fracturing of multi-strata for strong ground pressure control in extra-thick coal seams with hard roofs: Numerical simulation and case study. *Eng. Fract. Mech.* vol. 303, pp. 110129, 2024.

[12] X.Q Zhang, J.H Sun, C.D Liu, Q Sun. Synthesis comparative evaluation of hydrophobic polymer/surfactant fracturing fluids on methane adsorption-desorption and pore structure modifications in coal. *International Journal of Coal Science & Technology*, vol.12, pp. 86, 2025.

[13] K. Zhong, W.Z. Chen, W.S. Zhao, et al. Monitoring and evaluation of segmented hydraulic fracturing effect in rock burst prevention on hard roof of coal mine. *Journal of Central South University (Science and Technology)*, vol. 53, no. 7, pp. 2582-2593, 2022.

[14] X.B Zhang, J.F Li. Advancements and challenges of high-speed active flow control: Plasma actuators. *International Journal of Heat and Mass Transfer*, vol.252, pp.127481, 2025.

[15] B. Yu, T.J. Kuang, J.X. Yang, et al. Analysis of overburden structure and evolution characteristics of hard roof mining in extremely thick coal seam. *Coal Science and Technology*, vol. 51, no. 1, pp. 95-104, 2023.

[16] H.P. Kang, Y.J. Feng, Z. Zhang, et al. Hydraulic fracturing technology with directional boreholes for strata control in underground coal mines and its application. *Coal Science and Technology*, vol. 51, no. 1, pp. 31-44, 2023.

[17] W.L Shen, Z.Q Chen, M Wang, et al. Fracture characteristics and fracture interface buckling mechanism of cantilever rock mass under non-uniformly distributed load. *International Journal of Mining Science and Technology*, vol.12, 2025

[18] C.D Liu, R Zhang, Z.X Wang, et al. Research on the fire extinguishing performance of new gel foam for preventing and controlling the spontaneous combustion of coal gangue. *Environmental Science and Pollution Research*, vol. 30, pp. 88548-88562, 2023.

[19] S.K Zhao. Mechanism and application of force-structure cooperative prevention and control on rockburst with deep hole roof pre-blasting. *Journal of China Coal Society*, vol. 46, no. 11, pp. 3419-3432, 2021.

[20] Y.X Du, H. Zhang, L. Liang, et al. Application of machine vision in coal mine fully mechanized tunneling faces: a review. *IEEE Access*, vol. 11, pp. 102871-102898, 2023.

[21] J. Li, X. Zhang. Active flow control for supersonic aircraft: A novel hybrid synthetic jet actuator. *Sensors and Actuators A: Physical*. vol.302, pp. 111770, 2020.

[22] S.Y Jiang, J.H Zhang, K.L Diao, et al. Research advances in solvent extraction of lithium: the potential of ionic liquids. *Advanced Functional Materials*. vol. 35, no. 29, pp. 2423566, 2025.

[23] C.W Ling, Q. T Chen, W.Y Guo, et al. Study on overlying rock fissure and energy evolution law of high intensity mining working face adjacent to gob. *Safety in Coal Mines*, vol. 55, no. 12, pp. 48-56, 2024.

[24] M.S Gao, D. Xu, Y.L He, et al. Investigation on the near-far field effect of rock burst subject to the fracturing of thick and hard overburden. *Journal of Mining & Safety Engineering*, vol. 39, no. 2, pp. 215-226, 2022.

[25] K.Y Zhou, L.M Dou, J.Z Li, et al. Effect of extra-thick key strata on the static and dynamic stress of rockburst. *Journal of Mining & Safety Engineering*, vol. 41, no. 5, pp. 908-919, 2024.

[26] W.J Wang, F.Q Gao. Study of the evolution of mining-induced fractures with longwall face proceeds-insight from physical and numerical modeling. *Journal of Mining and Strata Control Engineering*, vol. 5, no. 2, pp. 17-26, 2023.

[27] F.Q. Gao, D. Stead, and H.P. Kang. Numerical Simulation of Squeezing Failure in a Coal Mine Roadway due to Mining-Induced Stresses. *Rock Mechanics and Rock Engineering*, vol. 48, no. 4, pp. 1635-1645, 2015.
[28] X. Zhang, Z.Wang, W. Chen. "Optimisation of synergistic ventilation between dust and gas in a gas tunnel," *Scientific Reports* ,vol.14, pp. 27582, 2024.
[29] M. Yang, S. Si, K. Zhang, et al. Bridging the relationship between physical exercise and mental health in adolescents based on network analysis. *Psy Ch journal*, vol. 13, no. 5, pp. 835-848, 2024.
[30] H. Rong, L. He, N. Li, et al. Technical research on surrounding rock control of roadways crossing collapse columns in strong mine pressure working faces. *Scientific Reports*. vol. 15, no. 1, 2025.

Acknowledgments

All authors contributed to this article. The authors express their sincere gratitude to the 1890 Coal Mine of Xinjiang Coking Coal Group for the invaluable support provided during the Engineering application of this study. Additionally, the constructive feedback provided by the editor and anonymous reviewers has greatly benefited the quality of this article.

Author Contributions

Conceptualization, Rui Wang., Haosen Wang; methodology, Rui Wang., Haosen Wang; software, Rui Wang., Haosen Wang. and Weiguang Zhang.; validation, Weiguang Zhang; formal analysis, Rui Wang., Haosen Wang. and Qiang Zhang.; data curation, Weiguang Zhang., Qiang Zhang; writing—original draft preparation, Rui Wang., and Haosen Wang.; writing—review and editing, Rui Wang., and Haosen Wang; project administration, Weiguang Zhang. All authors have read and agreed to the published version of the manuscript.

Funding

This research was funded by the Xinjiang Uygur Autonomous Region Tianchi Elite Talent Innovation Leadership Program, grant number 2024XGYTCYC03; the Urumqi City Hongshan Sci-Tech Innovation Elite Talents Youth Top Talents Program, grant number B241013004; the National Key Research and Development Program Young Scientists Project, grant number 2024YFC2910600; the Xinjiang Uygur Autonomous Region Key R&D Project Task Special-Department and Department Linkage Project, grant number 2022B01051-3; the Xinjiang Institute of Engineering Doctoral Start-up Fund, grant number 2023XGYBQJ14; and the Science and Technology Plan Project of Kekedala City, the Fourth Division of the Xinjiang Production and Construction Corps, grant number 2025ZR005.

Conflicts of Interest

The authors declare that they have no known competing financial interests or personal relationships that could have appeared to influence the work reported in this paper.

Additional information

Correspondence and requests for materials should be addressed to R.W. or HS.W.